


 Cite this: *RSC Adv.*, 2020, 10, 12547

# Spin relaxation induced by interfacial effects in n-GaN/MgO/Co spin injectors

 Xingchen Liu,<sup>a</sup> Ning Tang,<sup>\*ad</sup> Chi Fang,<sup>b</sup> Caihua Wan,<sup>\*b</sup> Shixiong Zhang,<sup>a</sup> Xiaoyue Zhang,<sup>a</sup> Hongming Guan,<sup>a</sup> Yunfan Zhang,<sup>a</sup> Xuan Qian,<sup>ce</sup> Yang Ji,<sup>ce</sup> Weikun Ge,<sup>a</sup> Xiufeng Han<sup>b</sup> and Bo Shen<sup>ad</sup>

Spin relaxation, affected by interfacial effects, is a critical process for electrical spin injection and transport in semiconductor-based spintronics. In this work, the electrical spin injection into n-GaN via n-GaN/MgO/Co tunnel barrier was realized, and the interface-related spin relaxation was investigated by both electrical Hanle effect measurement and time-resolved Kerr rotation (TRKR) spectrum. It was found that the spin relaxation caused by interfacial random magnetostatic field was nearly equal to the intrinsic contributions at low temperature (less than 80 K) and could be suppressed by smoother n-GaN/Co interface. When the interfacial random magnetostatic field was suppressed, the spin relaxation time extracted from the electrical injection process was still shorter than that in bulk conduction band, which was attributed to Rashba spin-orbit coupling (SOC) induced by the interface band bending in the depletion region. Due to thermal activation, luckily, the spin relaxation induced by the interfacial Rashba SOC was suppressed at temperatures higher than 50 K. These results illustrate that (1) spin relaxation time could be as long as 300 ps for GaN and (2) the influences of interfacial effects could be engineered to further prolong spin relaxation time, both of which shed lights on GaN-based spintronic devices with direct and wide bandgap.

Received 16th January 2020

Accepted 19th March 2020

DOI: 10.1039/d0ra00464b

[rsc.li/rsc-advances](http://rsc.li/rsc-advances)

## 1. Introduction

Spin injection into semiconductors is one of the key elements in developing spintronic devices, such as spin-polarized diode laser,<sup>1</sup> circular-polarized light-emitting diodes,<sup>2</sup> and spin field-effect transistors (FET).<sup>3-5</sup> Owing to relatively weak intrinsic spin-orbit coupling (SOC) in bulk GaN and as-induced long coherent length, bulk GaN and its low-dimensional structures are suitable for long spin transport and effective spin manipulation.<sup>6,7</sup> Spin-tunnelling barriers, such as MgO and Al<sub>2</sub>O<sub>3</sub> (ref. 8-12) or Schottky barriers,<sup>13-15</sup> are widely used to overcome the conductance mismatch and increase the spin injection efficiency. However, the localized interfacial states inside the tunnelling barriers may trap spin-polarized electrons<sup>13,16,17</sup> and block spin transport into bulk region. Furthermore, the

interfacial effects, including localized interfacial states, interfacial random magnetostatic field induced by roughness,<sup>18</sup> and the Rashba SOC field induced by the interface band bending,<sup>19,20</sup> significantly affect the spin relaxation process, whereas this topic has rarely been investigated systematically,<sup>13,16</sup> especially for wide-bandgap semiconductors.

Considering the spin relaxation time  $\tau_s$  is a critical parameter for spintronic devices, the spin relaxation processes induced by interfacial effects in the n-GaN/MgO/Co spin injectors were studied in this work. By comparing the  $\tau_s$  extracted under various temperatures and external magnetic field, different interface-related spin relaxation mechanisms during the spin injection process were identified. In addition,  $\tau_s$  extracted from the electrical spin injection process and dominated by interfacial effects is generally different from its bulk counterpart determined by optical method,<sup>21</sup> and their differences can reflect the influences of the interfacial effects. Therefore, besides the electrical Hanle effect measurements, here the time-resolved Kerr rotation (TRKR) spectrum was also adopted to measure the  $\tau_s$  of the conduction band electrons in the same bulk n-GaN.

## 2. Experiment

To investigate the spin relaxation processes induced by interfacial random magnetostatic field and interfacial band

<sup>a</sup>State Key Laboratory of Artificial Microstructure and Mesoscopic Physics, School of Physics, Peking University, Beijing 100871, China. E-mail: ntang@pku.edu.cn

<sup>b</sup>Beijing National Laboratory for Condensed Matter Physics, Institute of Physics, University of Chinese Academy of Sciences, Chinese Academy of Sciences, Beijing 100190, China. E-mail: wancaihua@iphy.ac.cn

<sup>c</sup>State Key Laboratory for Superlattices and Microstructures, Institute of Semiconductors, Chinese Academy of Sciences, Beijing 100083, China

<sup>d</sup>Frontiers Science Center for Nano-optoelectronics & Collaboration Innovation Center of Quantum Matter, Peking University, Beijing 100871, China

<sup>e</sup>College of Materials Science and Opto-Electronic Technology, College of Physical Sciences, University of Chinese Academy of Sciences, Beijing 100049, China



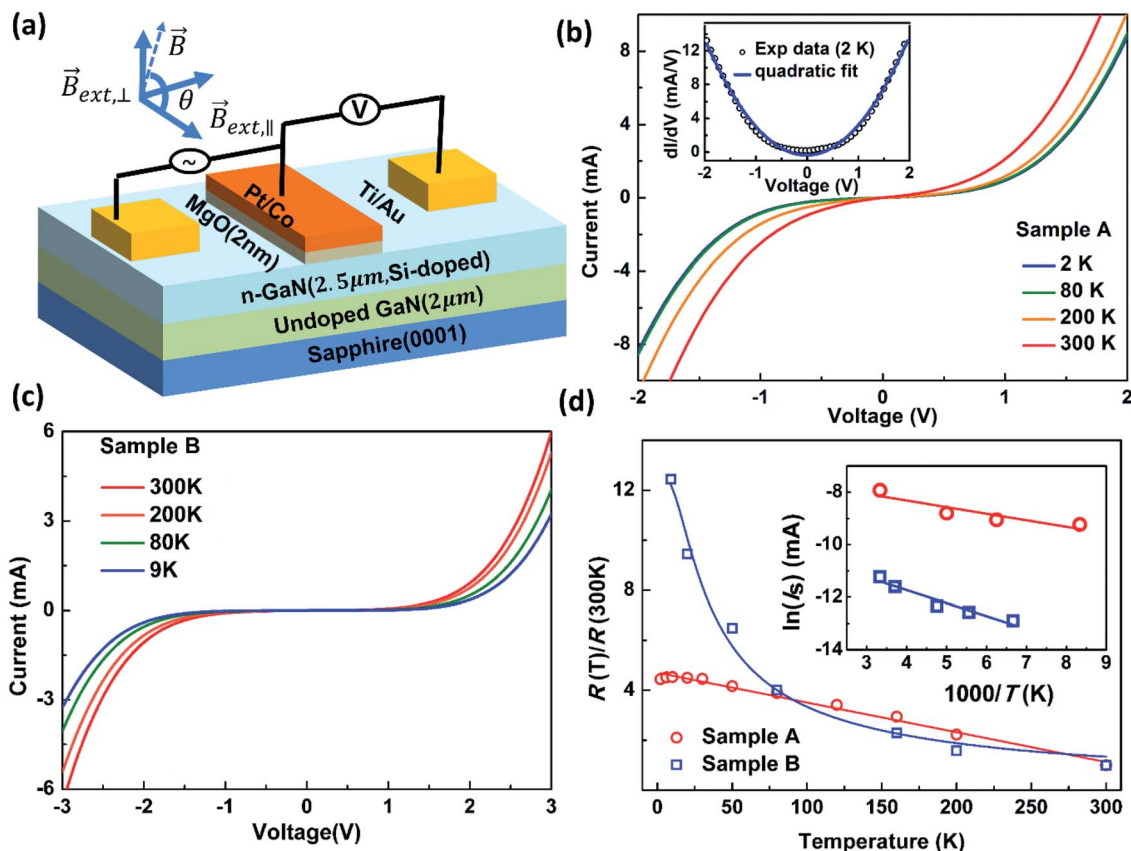


Fig. 1 (a) The schematic of the sample structures and setup of three-terminal Hanle effect measurements. (b) The  $I$ - $V$  characteristics of the injection circuit of sample A at various temperatures. The inset shows the differential conductance as a function of bias voltages. (c) The  $I$ - $V$  characteristics of the injection circuit of sample B at various temperatures. (d) Normalized zero-bias resistance as a function of temperature. The temperature dependence of saturation current is shown in the inset.

bending, two types of n-GaN/MgO/Co spin injectors were respectively fabricated in our experiments. The GaN layers of sample A (n-GaN, Si-doped:  $1 \times 10^{19} \text{ cm}^{-3}$ ) and sample B (n-GaN, Si-doped:  $1 \times 10^{17} \text{ cm}^{-3}$ ) were both grown by metal-organic chemical vapor deposition (MOCVD). Their stack structures consisted of  $2 \mu\text{m}$  undoped GaN and  $2.5 \mu\text{m}$  n-GaN grown on a  $c$ -axis sapphire substrate, as shown in Fig. 1(a). Then the samples were transferred into an ultrahigh vacuum magneto-sputtering system (ULVAC), where the tunnelling layer ( $2 \text{ nm}$  MgO) and ferromagnetic film ( $20 \text{ nm}$  Co) were deposited, followed by the deposition of  $10 \text{ nm}$  Pt to avoid oxidation. Finally, the three-terminal devices were fabricated by the standard UV photolithography and ion beam etching. Owing to the higher doping level, the n-GaN surface of sample A was rougher as indicated by atomic force microscope images ( $20 \mu\text{m} \times 20 \mu\text{m}$ ) which showed the root-mean-square roughness (RMS) of n-GaN was  $2.80 \text{ nm}$  and  $1.25 \text{ nm}$  for sample A and B, respectively. The rougher n-GaN/MgO interface caused by the rougher surface of n-GaN made the effect of the interfacial random magnetostatic field in sample A obvious as shown below. Instead, the wider depletion region in sample B caused by the lower doping level guaranteed the remarkable spin relaxation induced by interface band bending.

The low-temperature magnetotransport measurements were performed within a Physical Properties Measurement System (PPMS-9T, Quantum design). Keithley 2400, Keithley 6221 and a lock-in amplifier were used to conduct the  $I$ - $V$  and Hanle effect measurements. The same bulk GaN wafers without spin injectors (MgO/Co/Pt) was used for the TRKR measurements. The pump and probe beams were derived from the frequency-double output of a mode-locked Ti:Sapphire laser, and the beam energy varied from  $3.493 \text{ eV}$  to  $3.444 \text{ eV}$  to match the bandgap shift from  $9 \text{ K}$  to  $200 \text{ K}$ . The power ratio between the pump and probe beams approached to  $10 : 1$ , and the estimated density of photoexcited carriers was  $7.57 \times 10^{14} \text{ cm}^{-3}$  at  $9 \text{ K}$  and  $9.25 \times 10^{14} \text{ cm}^{-3}$  at  $200 \text{ K}$ , respectively. An external magnetic field was provided in the sample plane during the TRKR measurements.

### 3. Results and discussion

The  $I$ - $V$  measurements were conducted in the injection circuit by using two terminal geometry. The  $I$ - $V$  curves of sample A and sample B at various temperatures ( $T$ ) are shown in Fig. 1(b) and (c), both of which show a nonlinear and symmetric behaviour with varying the applied bias voltage. The differential conductance, which is deduced by taking the differential of  $I$ - $V$



curves with respect to voltage, exhibits a quadratic dependence on the bias voltage. Furthermore, the zero bias resistance ( $R(T)$ ) is derived by taking the reciprocal of conductance at zero voltage, which is usually used to analyze the tunnelling process.<sup>6,22</sup> The  $T$ -dependence of the normalized  $R(T)$  is shown in Fig. 1(d). For sample A, the  $R(T)$  shows a weak dependence on  $T$ , which evidences the direct tunnelling (phonon-irrelevant) dominated process.<sup>6,22</sup> In contrast, the  $R(T)$  of sample B shows a sharp and nonlinear  $T$ -dependence, indicating the sequential tunnelling through the localized interfacial states.<sup>23,24</sup> To further compare the tunnelling process, the tunnelling barriers of both samples are extracted. The  $I$ - $V$  curves at positive bias satisfy  $I = I_s \exp(eV/\eta k_B T)$  as  $eV \gg k_B T$  where  $I_s$ ,  $\eta$  and  $T$  are saturation current, ideal factor, and temperature, respectively. The saturation current can be expressed as  $I_s = AT^2 \exp(-E_b/k_B T)$  where  $E_b$  is the tunneling barrier.<sup>13,25</sup> It turns out that  $AT^2$  could be regarded as  $T$ -insensitive near room temperature<sup>13</sup> compared with the exponential term. Under this approximation,  $\ln(I_s)$  has a linear dependence on  $1/T$ . As shown in the inset of Fig. 1(d), by linearly fitting the dependence of  $\ln(I_s)$  on  $1/T$ , the tunneling barriers are derived as 22 meV and 43 meV for sample A and B, respectively. The higher tunnelling barrier of sample B can result from much lower doping level and indicates the stronger interfacial band bending.

Spin accumulation resulting from electrical spin injection was detected by a three-terminal geometry. The imbalanced spin polarization produces an additional electrochemical potential  $\Delta V_s$  (spin voltage). An external magnetic field (out-of-plane) perpendicular to the spin accumulation (Fig. 1(a)) can reduce  $\Delta V_s$  by Larmor precession, which is so-called the Hanle effect.<sup>18,26</sup> The dependence of  $\Delta V_s$  on the perpendicular magnetic field  $\vec{B}_{\text{ext},\perp}$  can be expressed as<sup>26</sup>

$$\Delta V_s(B) = \Delta V_s(0)/[1+(\omega\tau_s)^2] \quad (1)$$

where  $\omega$ , the frequency of Larmor precession, has a linear dependence on  $B_{\text{ext},\perp}$  via  $\omega = g\mu_B B_{\text{ext},\perp}/\hbar$ , and  $g$  is the effective Landé  $g$ -factor in n-GaN ( $g = 1.95$  in bulk GaN<sup>27,28</sup>),  $\mu_B$  is the Bohr magneton and  $\hbar$  is the reduced Planck's constant. Considering the interests were focused on the behaviour near zero bias current, only an AC current source was used to inject spin-polarized electrons, as shown in Fig. 1(a).

Then the variation of  $\Delta V_s$  under  $\vec{B}_{\text{ext},\perp}$  was detected by a lock-in amplifier. The typical Hanle effect curves of sample A and sample B are shown in Fig. 2(a) and 4(a), respectively, and  $\tau_s$  can be extracted from the Hanle curves.

Besides of the Hanle effect, the inverted Hanle effect<sup>18,29</sup> responding to the in-plane external magnetic field  $B_{\text{ext},\parallel}$  was observed in sample A while absent in sample B, as shown in

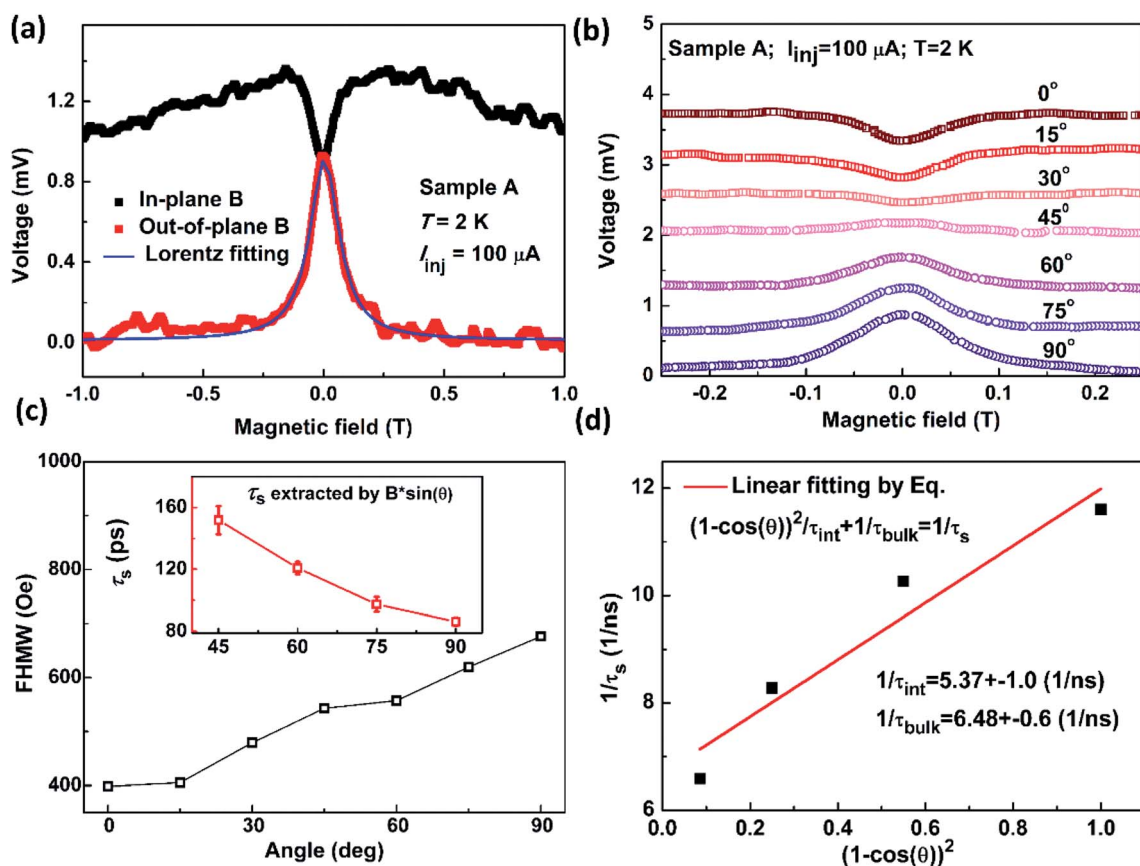


Fig. 2 (a) The Hanle and inverted Hanle curves in sample A at 2 K. (b) The angle-dependent Hanle and inverted Hanle curves in sample A at 2 K. (c) The extracted FWHM at various angles, and the inset shows the spin relaxation time extracted from the Hanle curves ( $\theta \geq 45^\circ$ ). (d) The spin relaxation rate  $1/\tau_{\text{int}}$  and  $1/\tau_{\text{bulk}}$  are extracted by linear fitting  $1/\tau_s$  against  $(1 - \cos(\theta))^2$ .



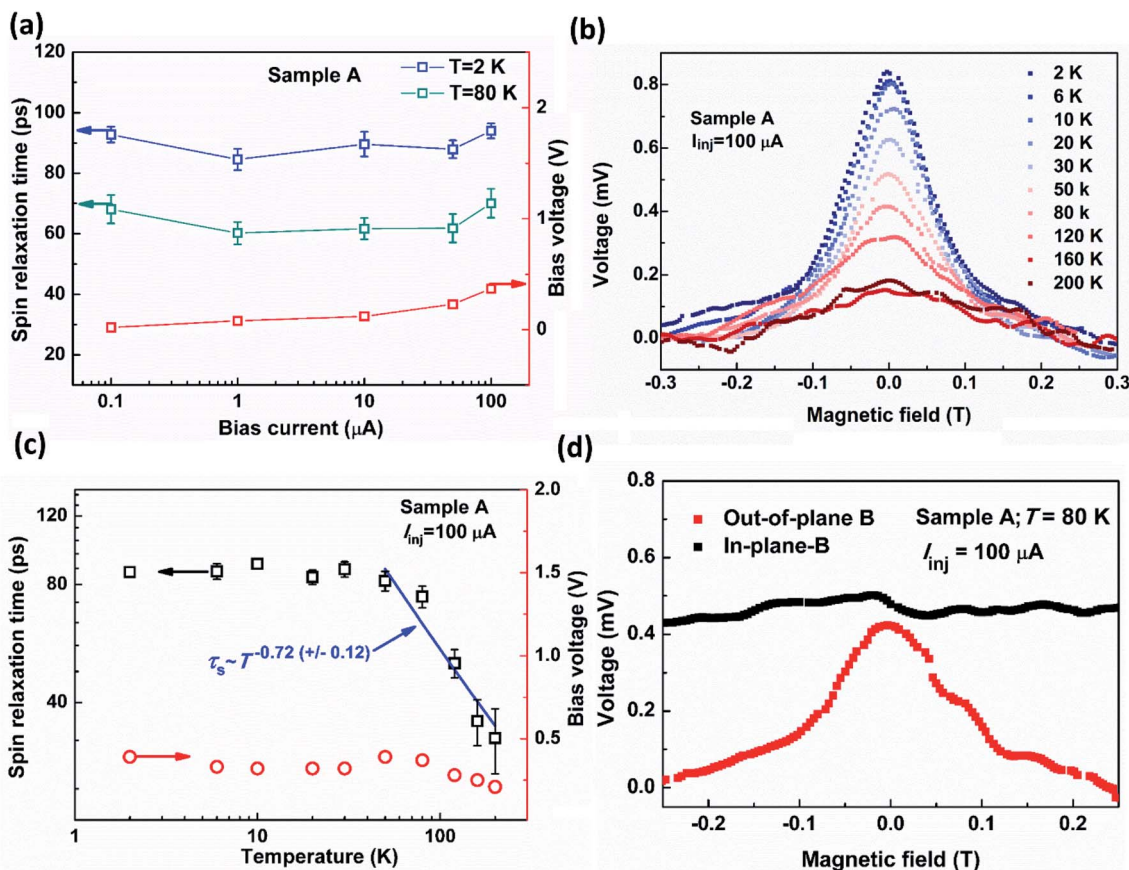


Fig. 3 (a) The bias current-dependent  $\tau_s$  and bias voltage in sample A. (b) The temperature-dependent Hanle curves under  $I_{inj} = 100 \mu\text{A}$ . (c) The temperature-dependent  $\tau_s$  extracted from Hanle curves and bias voltage under  $I_{inj} = 100 \mu\text{A}$ . (d) The Hanle curve in sample A at 80 K, while the inverted Hanle curve is vanished.

Fig. 2(a) and 4(a). According to ref. 18, larger roughness of the MgO/Co interface (caused by rougher GaN surface for sample A) results in an interfacial random magnetostatic field  $\vec{Q}_{FM}$  which can accelerate spin relaxation process. The spin relaxation rate caused by  $\vec{Q}_{FM}$  can be expressed as:<sup>28</sup>

$$1/\tau_{s,int} \propto \langle \vec{Q}_{FM}^2(\vec{r}) \rangle \quad (2)$$

where  $\langle \vec{Q}_{FM}(\vec{r}) \rangle$  represents the interfacial random magnetostatic field averaged over the electron position during the injection process. The in-plane parallel field can stabilize the spin accumulation from relaxing and prolong its relaxation time and finally leads to a positive magnetic resistance (MR) as shown in Fig. 2(a). These in-plane and out-of-plane magnetic field dependence of  $\Delta V_s$  demonstrate build-up of spin accumulation inside n-GaN and rule out other effects, such as impurity-assisted tunnelling magnetoresistance that should be isotropic with respect to the field directions.<sup>23</sup> In addition, the absence of the inverted Hanle effect in sample B also indicated the spin relaxation mechanism caused by  $\vec{Q}_{FM}$  could be ignored for sample B whose interfacial roughness was smaller than sample A.

Sample A was then utilized to investigate spin relaxation processes influenced by  $\vec{Q}_{FM}$  (the interfacial random magnetostatic field due to interfacial roughness). As shown in Fig. 2(b), the

Hanle and inverted Hanle curves were measured at different angle  $\theta$  between magnetic field and sample plane.  $\theta$  was defined as shown in Fig. 1(a). As  $\theta$  changed from  $90^\circ$  to  $0^\circ$ , the effect dominating spin relaxation changed from Hanle effect to inverted Hanle effect. Thus the spin voltages reversed sign with the decreased  $\theta$ . The full width at half maximum (FWHM) of the Hanle curve is proportional to the spin relaxation rate ( $1/\tau_s$ ) according to eqn (1). As shown in Fig. 2(c), the extracted FWHM ( $\tau_s$ ) increases (decreases) with increasing  $\theta$ . Actually, the effective external magnetic field  $B_{ext,\perp}^{eff} = B_{ext}\sin(\theta)$  is used to extract  $\tau_s$  from the Hanle curves ( $\theta \geq 45^\circ$ ). The extracted  $\tau_s$  decreases from 152 ps to 86 ps shown in the inset of Fig. 2(c).

As seen in Fig. 1(a), considering the suppression effect of  $B_{ext,\parallel}$ , the  $\theta$ -dependence of  $\langle \vec{Q}_{FM}^2(\vec{r}) \rangle$  could be expressed as  $\langle \vec{Q}_{FM}^2(\vec{r}) \rangle \propto (1 - \cos(\theta))^2$ . Combining eqn (2), the angle-dependent spin relaxation rate ( $1/\tau_s$ ) can be given as  $1/\tau_s = (1 - \cos(\theta))^2/\tau_{int} + 1/\tau_{bulk}$  where  $1/\tau_{int}$  and  $1/\tau_{bulk}$  correspond to the spin relaxation rate induced by  $\vec{Q}_{FM}$  and spin relaxation rate induced by bulk GaN, respectively. As shown in Fig. 2(d), by linearly fitting the dependence of  $1/\tau_s$  on  $(1 - \cos(\theta))^2$ , the spin relaxation rates are derived as  $1/\tau_{int} = 5.37$  (1/ns) and  $1/\tau_{bulk} = 6.48$  (1/ns). The results indicate that the spin relaxation caused by  $\vec{Q}_{FM}$  was comparable to the intrinsic contributions of bulk GaN at 2 K.



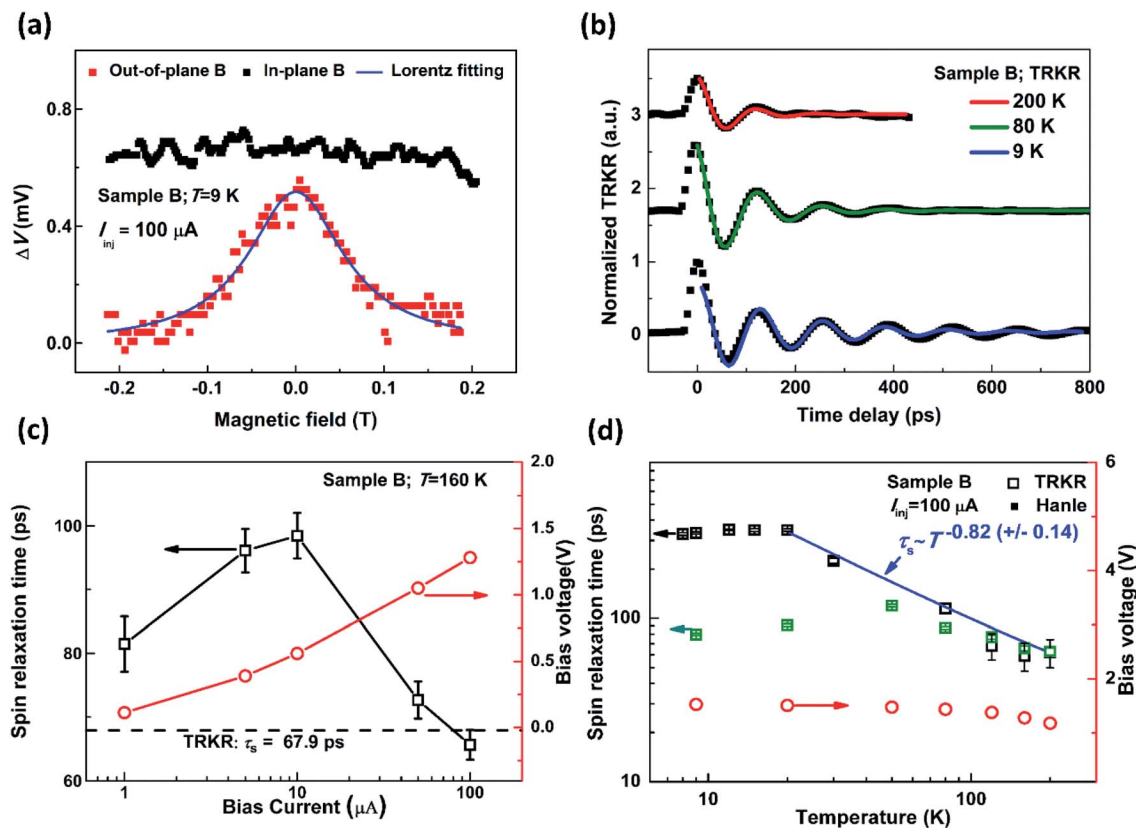


Fig. 4 (a) The Hanle curve and vanished inverted Hanle curve in sample B at 9 K. (b) The TRKR signals under an external magnetic field at various temperatures. (c) The bias current-dependent  $\tau_s$  and bias voltage at 160 K. The corresponding  $\tau_s$  extracted from TRKR is also shown. (d)  $\tau_s$  extracted by Hanle curves under  $I_{inj} = 100 \mu A$  and TRKR measurements in sample B at various temperatures.

Furthermore, the  $T$ -dependent  $\tau_s$  was extracted by electrical Hanle effect measurements in sample A. Firstly, in order to exclude influence of the localized interfacial states, the dependence of  $\tau_s$  on bias current was measured. As shown in Fig. 3(a),  $\tau_s$  hardly depended on the bias current, which confirmed the extracted  $\tau_s$  was not affected by localized interfacial states. If those localized interfacial states were involved in spin transport and relaxation, noticeable bias-dependent  $\tau_s$  would have been expected as reported in ref. 13 and 16. Then the Hanle curves were obtained at various temperatures under the same bias current. As shown in Fig. 3(b), the spin voltages  $\Delta V_s$  of Hanle curves decreased gradually with increasing  $T$ , and the extracted  $\tau_s$  was shown in Fig. 3(c). The spin relaxation mechanism has been extensively studied in wurtzite bulk GaN, and the Dyakonov-Perel (DP) spin relaxation mechanism originating from the bulk SOC is regarded as the dominant one.<sup>28,30,31</sup> In the DP scenario, the dependence of  $\tau_s$  on  $T$  satisfies<sup>28</sup>

$$\tau_{s,bulk} \propto 1/[(k_1 T + k_3 T^3)\tau_p] \quad (3)$$

where  $\tau_p$  is the momentum scattering time,  $k_1$  and  $k_3$  represent the coefficients related to Rashba and Dresselhaus SOC terms, respectively. With increasing  $T$ , shown in Fig. 3(c), the extracted  $\tau_s$  was almost constant at temperatures lower than 80 K. At higher temperatures,  $\tau_s$  decreased rapidly, and satisfied  $\tau_s \propto T^{-0.72 \pm 0.12}$ . The weak  $T$ -dependence of  $\tau_s$  could be attributed to

$\vec{Q}_{FM}$  induced spin relaxation in low temperature region. As shown in Fig. 3(d), the inverted Hanle effect are almost negligible at 80 K, which means the dominant spin relaxation mechanism changed to DP mechanism of bulk GaN in high-temperature region. The Rashba SOC is the major contributing term for the DP mechanism in bulk GaN,<sup>28</sup> and the  $T$ -dependence of  $\tau_s$  satisfies  $\tau_s \propto T^{-1}$ . The extracted  $\tau_s \propto T^{-0.72 \pm 0.12}$ , which was close to the theoretical prediction. Their discrepancy might arise due to the  $T$ -independent spin relaxation induced by  $\vec{Q}_{FM}$ . Since the bias voltage was kept nearly constant at different temperatures, shown in Fig. 3(c), the influence of the electron kinetic energy could be safely excluded.<sup>32</sup>

In sample A with very high doping level and large roughness, the above data indicated interface random magnetostatic field remarkably influenced spin relaxation. In the following part, instead, sample B with lower doping density and wider Schottky barrier was utilized to investigate the spin relaxation process influenced by interface band bending. Besides of the electrical Hanle effect measurements, the TRKR was used to measure the  $\tau_s$  of the same bulk n-GaN with sample B for comparison. In addition, due to the much higher background carrier density, the signal-to-noise ratio of the TRKR results was too low to accurately extract a reliable spin relaxation time in the n-GaN of sample A. Owing to the absence of the spin injector (MgO/Co/



Pt), the spin relaxation is not affected by interface band bending effect in the TRKR measurements. The TRKR signal is shown in Fig. 4(b) at various temperatures, where a double exponential cosine damped function  $[A_1 \exp(-t/\tau_c) + A_2 \exp(-t/\tau_s) \cos(\omega t)]$  was used to extract  $\tau_s$  where  $\tau_c$  represented the recombination time of photon-generated carriers.<sup>28</sup> As shown in Fig. 4(d), the  $T$ -dependence of  $\tau_s$  extracted from the TRKR satisfied  $\tau_s \propto T^{-0.82 \pm 0.14}$  at  $T$  higher than 20 K. With increased  $T$ , the  $\tau_s$  increased slightly at  $T$  below 20 K, which was attributed to the  $T$ -dependent momentum scattering time.<sup>33</sup>

According to the DP spin relaxation mechanism, the lightly doped bulk GaN (sample B) has a longer  $\tau_s$  than the highly doped one (sample A).<sup>30</sup> This feature will lead a more sensitive dependence on  $\vec{Q}_{\text{FM}}$  for sample B during the electrical spin injection process. However, as shown in Fig. 4(a), the  $\vec{Q}_{\text{FM}}$ -related inverted Hanle effect is absent in sample B at 9 K, which confirmed that the  $\vec{Q}_{\text{FM}}$  induced spin relaxation is suppressed in sample B by the smoother n-GaN/Co interface.

Moreover, the dependence of  $\tau_s$  on bias current was measured to check influence of localized interfacial states.<sup>16</sup> As seen in Fig. 4(c),  $\tau_s$  of sample B extracted from Hanle effect was sensitive to the bias current and became much longer under low bias current, which was different from the case of sample A. In sample A with heavy doping level, Schottky barrier was thin and therefore the MgO barrier dominated transport. However, in sample B with much lower doping level, Schottky barrier became much thicker as well and its influence could not be ignored anymore.

Considering multistep sequential tunnelling process inside Schottky barrier region *via* the localized interfacial states as reported in ref. 13, the effective  $\tau_s$  extracted from Hanle measurement should be actually an averaged spin relaxation time  $\tau_{\text{int}}$  of the localized interfacial states and  $\tau_{\text{bulk}}$  of the bulk.<sup>13,16</sup> Fortunately,  $\tau_s$  is close to  $\tau_{\text{int}}$  under low negative bias voltages and becomes closer to  $\tau_{\text{bulk}}$  under higher negative bias voltages due to different tunnelling channels under different bias conditions.<sup>13,16,17</sup> Under the framework of DP mechanism, the spin relaxation is mainly attributed to the fluctuation of wave vector  $\vec{k}$ -dependent effective magnetic field  $\vec{Q}_{\vec{k}}$  induced by SOC.<sup>28</sup> Owing to the protection effect of the potential well surrounding the interfacial defects, the fluctuation is suppressed and  $\tau_{\text{int}}$  is normally longer than  $\tau_{\text{bulk}}$ ,<sup>13,16</sup> which results in the longer  $\tau_s$  under low bias voltages as in our case.

As shown in Fig. 4(c), however,  $\tau_s$  measured by Hanle effect approached to the TRKR value under a larger bias current (such as  $\tau_s$  measured at 100  $\mu\text{A}$ ). This feature indicated that the spin-polarized electrons escaped from the localized interfacial states into bulk region under large bias and the measured  $\tau_s$  from Hanle effect also tended to be its bulk value. In addition, the results also confirmed that the decrease of  $\tau_s$  at large bias voltage could not be attributed to the electron kinetic energy effect. That would make the  $\tau_s$  extracted from the electrical Hanle effect much shorter than that in bulk conduction band (extracted by TRKR) under 100  $\mu\text{A}$ , which is opposite to our experimental results.

The  $T$ -dependent  $\tau_s$ , which was extracted from electrical injection process under the large bias current  $I_{\text{inj}} = 100 \mu\text{A}$ , is

shown in Fig. 4(d). At  $T$  below 50 K,  $\tau_s$  extracted from Hanle curves was shorter than that measured by TRKR, and approached identical with the TRKR results at higher temperatures. According to the aforementioned discussion, the spin relaxation induced by the mechanism of interfacial random magnetostatic field has been excluded for sample B due to absence of the inverted Hanle effect. It is worth noting that the interfacial Rashba SOC induced by band bending has been studied experimentally and theoretically based on MOSFET structure.<sup>19,20</sup> Accordingly, we attributed the much shorter  $\tau_s$  than the TRKR result at low temperatures to the interfacial Rashba SOC induced by band bending in the depletion region. In more detail, interfacial inversion symmetry breaking greatly enhanced interfacial Rashba SOC and thus spin relaxation in this depletion region, which made the  $\tau_s$  extracted from the electrical injection process much shorter than that in bulk conduction band. Considering the  $T$ -independent bias-voltage, as shown in Fig. 4(d), the interface band bending induced Rashba SOC could also be regarded as  $T$ -independent. However, as indicated in ref. 16, the characteristic leakage time  $\tau_{\text{L}}^{\text{S}}$  will introduce a temperature-dependent effect to  $\tau_s$ . A relevant parameter  $\tau_{\text{L}}^{\text{S}}$  can be defined as the time of electron escaping from the interfacial depletion region into the GaN conduction band in our case. It has been observed that  $\tau_{\text{L}}^{\text{S}}$  (the carrier backward escape time  $\tau_{\text{n}}$ ) decrease (increase) with temperature due to the thermal activation.<sup>16</sup> The shorter  $\tau_{\text{L}}^{\text{S}}$  guarantees the weaker influence of the interface band bending on spin relaxation process. As a result, the effect of interface band bending on spin relaxation was eliminated at high temperatures, which is consistent with results in Fig. 4(d). Similarly, the nearly  $T$ -independent bias voltage also indicated that the effect of the electron kinetic energy could also be excluded.

## 4. Conclusions

In conclusion, the electrical spin injection into bulk n-GaN was demonstrated at temperatures from 2 K to 200 K, and spin relaxation related with interfacial effects during the electrical injection process was studied. In particular, the spin relaxation process induced by interfacial random magnetostatic field was comparable to the intrinsic contribution at low temperature for heavily doped GaN, and this effect could be suppressed by smoothening n-GaN interface for lightly doped samples. The interfacial Rashba SOC caused by band bending for the lightly doped GaN greatly enhanced spin relaxation at low temperature and could be eliminated by thermal activation at high temperatures and large bias condition both of which can help electrons escape from the interfacial depletion region. These results indicated some principles, (1) smooth surface to lower interfacial random magnetostatic field and (2) large bias condition and high temperatures to help spin-polarized electrons escape from interfacial depletion region, to engineer GaN/MgO/Co spin injectors to realize longer spin relaxation time, which could advance the development of spintronics based on wide-bandgap semiconductors.



## Conflicts of interest

There are no conflicts to declare.

## Acknowledgements

The authors would like to thank professor Yuan Lu for helpful discussions. This work was supported by National Key Research and Development Program of China (No. 2018YFB0406603, 2017YFA0206200, and 2016YFA0301202), the National Natural Science Foundation of China (No. 61574006, 61522401, 11974398, 61927806, 61521004, 11634002 and 11674311) and K. C. Wong Education Foundation, China. C. H. Wan also appreciates financial support from Youth Innovation Promotion Association, CAS (Grant No. 2020008).

## Notes and references

- 1 A. Bhattacharya, M. Z. Baten, I. Iorsh, T. Frost, A. Kavokin and P. Bhattacharya, *Phys. Rev. Lett.*, 2017, **119**(6), 067701.
- 2 J. Y. Chen, C. Y. Ho, M. L. Lu, L. J. Chu, K. C. Chen, S. W. Chu, W. Chen, C. Y. Mou and Y. F. Chen, *Nano Lett.*, 2014, **14**, 3130–3137.
- 3 S. Datta and B. Das, *Appl. Phys. Lett.*, 1990, **56**, 665–667.
- 4 H. C. Koo, J. H. Kwon, J. Eom, J. Chang, S. H. Han and M. Johnson, *Science*, 2009, **325**, 1515–1518.
- 5 P. Chuang, S.-C. Ho, L. W. Smith, F. Sfigakis, M. Pepper, C.-H. Chen, J.-C. Fan, J. P. Griffiths, I. Farrer, H. E. Beere, G. A. C. Jones, D. A. Ritchie and T.-M. Chen, *Nat. Nanotechnol.*, 2015, **10**, 35–39.
- 6 A. Bhattacharya, M. Z. Baten and P. Bhattacharya, *Appl. Phys. Lett.*, 2016, **108**(4), 042406.
- 7 T.-E. Park, Y. H. Park, J.-M. Lee, S. W. Kim, H. G. Park, B.-C. Min, H.-J. Kim, H. C. Koo, H.-J. Choi, S. H. Han, M. Johnson and J. Chang, *Nat. Commun.*, 2017, **8**(1), 1–7.
- 8 E. I. Rashba, *Phys. Rev. B: Condens. Matter Mater. Phys.*, 2000, **62**, R16267–R16270.
- 9 A. Fert and H. Jaffrès, *Phys. Rev. B: Condens. Matter Mater. Phys.*, 2001, **64**(18), 184420.
- 10 V. F. Motsnyi, J. De Boeck, J. Das, W. Van Roy, G. Borghs, E. Goovaerts and V. I. Safarov, *Appl. Phys. Lett.*, 2002, **81**, 265–267.
- 11 V. F. Motsnyi, P. Van Dorpe, W. Van Roy, E. Goovaerts, V. I. Safarov, G. Borghs and J. De Boeck, *Phys. Rev. B: Condens. Matter Mater. Phys.*, 2003, **68**(24), 245319.
- 12 C. Fang, C. H. Wan, B. S. Yang, J. Y. Qin, B. S. Tao, H. Wu, X. Zhang, X. F. Han, A. Hoffmann, X. M. Liu and Z. M. Jin, *Phys. Rev. B: Condens. Matter Mater. Phys.*, 2017, **96**(13), 134421.
- 13 L. Huang, H. Wu, P. Liu, X. M. Zhang, B. S. Tao, C. H. Wan, Y. Yan and X. F. Han, *Appl. Phys. Lett.*, 2018, **113**(22), 222402.
- 14 A. T. Hanbicki, O. M. J. van 't Erve, R. Magno, G. Kioseoglou, C. H. Li, B. T. Jonker, G. Itkos, R. Mallory, M. Yasar and A. Petrou, *Appl. Phys. Lett.*, 2003, **82**, 4092–4094.
- 15 A. T. Hanbicki, B. T. Jonker, G. Itkos, G. Kioseoglou and A. Petrou, *Appl. Phys. Lett.*, 2002, **80**, 1240–1242.
- 16 M. Tran, H. Jaffrès, C. Deranlot, J. M. George, A. Fert, A. Miard and A. Lemaître, *Phys. Rev. Lett.*, 2009, **102**(3), 036601.
- 17 A. Jain, J. C. Rojas-Sanchez, M. Cubukcu, J. Peiro, J. C. Le Breton, E. Prestat, C. Vergnaud, L. Louahadj, C. Portemont, C. Ducruet, V. Baltz, A. Barski, P. Bayle-Guillemaud, L. Vila, J. P. Attané, E. Augendre, G. Desfonds, S. Gambarelli, H. Jaffrès, J. M. George and M. Jamet, *Phys. Rev. Lett.*, 2012, **109**(10), 106603.
- 18 S. P. Dash, S. Sharma, J. C. Le Breton, J. Peiro, H. Jaffrès, J. M. George, A. Lemaître and R. Jansen, *Phys. Rev. B: Condens. Matter Mater. Phys.*, 2011, **84**(5), 054410.
- 19 T. Matsuyama, R. Kürsten, C. Meißner and U. Merkt, *Phys. Rev. B: Condens. Matter Mater. Phys.*, 2000, **61**, 15588–15591.
- 20 S. Lamari, *Phys. Rev. B: Condens. Matter Mater. Phys.*, 2001, **64**(24), 245340.
- 21 C. Y. Hu, K. Morita, H. Sanada, S. Matsuzaka, Y. Ohno and H. Ohno, *Phys. Rev. B: Condens. Matter Mater. Phys.*, 2005, **72**(12), 121203.
- 22 S. Jahangir, F. Doğan, H. Kum, A. Manchon and P. Bhattacharya, *Phys. Rev. B: Condens. Matter Mater. Phys.*, 2012, **86**(3), 035315.
- 23 O. Txoperena, Y. Song, L. Qing, M. Gobbi, L. E. Hueso, H. Dery and F. Casanova, *Phys. Rev. Lett.*, 2014, **113**(14), 146601.
- 24 J.-Y. Park, S.-heon C. Baek, S.-Y. Park, Y. Jo and B.-G. Park, *Appl. Phys. Lett.*, 2015, **107**(18), 182407.
- 25 S. M. Sze, *Semiconductor devices: physics and technology*, John Wiley & sons, 2008, John Wiley & Sons, INC., New York, 3rd edn, 2012, ch. 7, pp. 228–238.
- 26 S. P. Dash, S. Sharma, R. S. Patel, M. P. de Jong and R. Jansen, *Nature*, 2009, **462**, 491–494.
- 27 A. V. Rodina and B. K. Meyer, *Phys. Rev. B: Condens. Matter Mater. Phys.*, 2001, **64**(24), 245209.
- 28 J. H. Buß, J. Rudolph, F. Natali, F. Semond and D. Hägele, *Phys. Rev. B: Condens. Matter Mater. Phys.*, 2010, **81**(15), 155216.
- 29 A. Jain, L. Louahadj, J. Peiro, J. C. Le Breton, C. Vergnaud, A. Barski, C. Beigné, L. Notin, A. Marty, V. Baltz, S. Auffret, E. Augendre, H. Jaffrès, J. M. George and M. Jamet, *Appl. Phys. Lett.*, 2011, **99**(16), 162102.
- 30 J. H. Buß, J. Rudolph, S. Starosielec, A. Schaefer, F. Semond, Y. Cordier, A. D. Wieck and D. Hägele, *Phys. Rev. B: Condens. Matter Mater. Phys.*, 2011, **84**(15), 153202.
- 31 J. H. Buß, J. Rudolph, F. Natali, F. Semond and D. Hägele, *Appl. Phys. Lett.*, 2009, **95**(19), 192107.
- 32 S. Krishnamurthy, M. van Schilfgaarde and N. Newman, *Appl. Phys. Lett.*, 2003, **83**, 1761–1763.
- 33 C. Adelman, X. Lou, J. Strand, C. J. Palmström and P. A. Crowell, *Phys. Rev. B: Condens. Matter Mater. Phys.*, 2005, **71**(12), 121301.

